Journal of Energy Storage 68 (2023) 107769

Contents lists available at ScienceDirect

Journal of Energy Storage

journal homepage: www.elsevier.com/locate/est

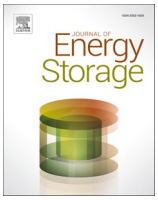

Research papers

# A novel niobium (oxy)nitride-$BaCe_{0.7}Zr_{0.1}Y_{0.2}O_{3-\delta}$ composite electrode for Proton Ceramic Membrane Reactors (PCMRs)

Vanessa C.D. Graça *, Laura I.V. Holz, Allan J.M. Araújo, Francisco J.A. Loureiro, Duncan P. Fagg *

*TEMA-Centre for Mechanical Technology and Automation, Department of Mechanical Engineering, University of Aveiro, 3810-193 Aveiro, Portugal*
*LASI-Intelligent Systems Associate Laboratory, Portugal*

ARTICLE INFO

*Keywords:*
Proton ceramic membrane reactor (PCMR)
Yttrium-doped barium zirconate-cerate (BCZY)
Transition metal nitride (TMN)
Niobium (oxy)nitride
Electrochemical impedance spectroscopy (EIS)

ABSTRACT

The necessity to accelerate green and low carbon technologies, to mitigate the pending energetic crisis, potentiates the urgent search for alternative energy transfer methods. In this regard, Proton Ceramic Membrane Reactors (PCMRs) have shown great potential as a clean alternative for both energy production and the electrochemical synthesis of a wide range of chemical products. One of the most important is that of ammonia, where recent literature has demonstrated the potential use of PCMRs to either synthesize this chemical product or to use it as a fuel, and where suitable new electrodes must be developed. Hence, this work investigates the use of niobium (oxy)nitride ($NbN_xO_y$) in combination with proton ceramic conducting materials, as a new category of composite electrode for PCMRs applications. To achieve this goal, firstly, the chemical compatibility of the $NbN_xO_y$ phase with the well-known proton conducting perovskite, yttrium-doped barium cerate ($BaCe_{0.9}Y_{0.1}O_{3-\delta}$, BCY10), was assessed. By X-ray powder diffraction, $BaCe_{0.7}Zr_{0.1}Y_{0.2}O_{3-\delta}$ (BCZY712) was shown to be chemically stable with the $NbN_xO_y$ phase, surviving up to 850 °C, thus, facilitating the production of an electrolyte supported composite electrode film based on BCZY712-$NbN_xO_y$ (40–60 vol%). Thermogravimetric experiments combined with X-ray diffraction were also made to assess the thermal stability of the $NbN_xO_y$ material in both $N_2$ and 2 % $H_2/N_2$ atmospheres, revealing that $NbN_xO_y$ decomposes into its parent oxide in $N_2$, while retaining the pure (oxy)nitride phase in the more reducing conditions. The polarization behavior of the BCZY712-$NbN_xO_y$ composite electrode was evaluated by electrochemical impedance spectroscopy under different gaseous conditions of $H_2/N_2$ and $NH_3$ atmospheres. The overall electrode mechanism was tentatively explained by three main steps, including i) proton incorporation/water release or adsorption/desorption of water, ii) gaseous hydrogen adsorption/desorption, and iii) interfacial transfer reaction of either protons or oxygen-ion vacancies. To the best of our knowledge, this is the first work that reports a detailed chemical compatibility study of niobium (oxy) nitride with a protonic ceramic matrix, while also outlining a detailed electrode mechanism under prospective conditions of hydrogenation/de-hydrogenation of ammonia.

## 1. Introduction

The current requirements of low carbon strategies have led many companies to announce low-carbon or net zero strategies, in which the use of alternative fuels, such as hydrogen ($H_2$) may play a crucial role. Nonetheless, despite the potential of the hydrogen economy compared to the current fossil fuel economy, several challenges remain to be addressed regarding the storage and distribution of hydrogen. Hydrogen's volatility, very low flash point, invisible flame, and low volumetric energy density, pose several complications for storing and transporting energy in the form of pure hydrogen, with the necessary infrastructure based on pressurized hydrogen distributed in pipes, also requiring prohibitively large investments [1–3].

On the other hand, a potential alternative is that of ammonia ($NH_3$), which, like hydrogen, does not contain carbon in its structure, thereby avoiding the emission of $CO_2$ upon its combustion, while also being easy to liquefy at relatively low pressure (1030 kPa) at ambient temperature; a key property that hydrogen cannot provide [3,4]. This makes the

* Corresponding authors at: TEMA-Centre for Mechanical Technology and Automation, Department of Mechanical Engineering, University of Aveiro, 3810-193 Aveiro, Portugal.
*E-mail addresses:* vanessagraca@ua.pt (V.C.D. Graça), duncan@ua.pt (D.P. Fagg).

https://doi.org/10.1016/j.est.2023.107769
Received 25 November 2022; Received in revised form 5 May 2023; Accepted 16 May 2023
Available online 25 May 2023

storage and transportation of compressed liquid ammonia much simpler and safer compared to hydrogen and can provide a fuel with a superior volumetric density (11.3 GJ $m^{-3}$) than that of compressed natural gas (10.4 GJ $m^{-3}$) or gaseous (2.1 GJ $m^{-3}$) or liquid (8.5 GJ $m^{-3}$) hydrogen. Ammonia is also an important raw chemical for producing fertilizers, where the well-established infrastructures and facilities for transport and storage around the world would boost the usage of ammonia as a potential clean energy source in the near future [1–3,5,6].

Proton Ceramic Membrane Reactors (PCMRs) have gained increasing attention, due to their capability to operate under ammonia-based fuels in fuel cell mode to produce electricity [4,7,8]. Conversely, they can also be operated in the inverse direction to produce ammonia directly from electricity and steam or hydrocarbons at ambient pressure [4,9,10]. This possibility can present several advantages when compared to the traditional Haber-Bosch (HB) process, such as a significant cost saving, as well as the elimination of the large carbon footprint of the standard natural gas route of the HB process [4,9,10].

The flexibility of these devices for both hydrogenation and de-hydrogenation of ammonia is permitted using a solid-state proton-conducting electrolyte membrane [4,9,10]. Typical electrolytes are based on perovskite proton conductors with very high protonic conductivity, such as doped barium cerate/zirconates (*e.g.*, $10^{-3}$ S $cm^{-1}$ at 400 °C [11–14]), which can have the ability to operate in very low humidity conditions (*e.g.*, $p_{H2O} \leq 10^{-4}$ atm), an essential requirement to avoid ammonium ($NH_4^+$) formation. Nonetheless, for both ammonia-based applications, the critical limitation, to date, is based on the lack of suitable electrode materials. For example, in the case of anodes for ammonia fuel oxidation, current Ni-based cermet materials suffer from poor chemical stability in $NH_3$-containing fuels, yielding phase nitrification to $Ni_3N$ (nickel nitride), with a potentially detrimental effect with respect to their catalytic behavior for ammonia oxidation [15–17]. Equally, in the case of ammonia formation electrodes, reported Faradaic efficiencies remain low (below 10–15 %), mainly due to the poor catalytic activity/selectivity towards $N_2$ reduction reaction [4,9,10,18].

Hence, alternative electrode materials are urgently required for these technologies. In this regard, recent works on transition metal (oxy)nitrides, based on vanadium, niobium, chromium, zirconium, *etc.*, have been shown that these materials are stable in reducing conditions, while also being attractive as electrocatalysts for electrochemical ammonia synthesis [19–22]. However, with respect to their use in PCMRs, only one example was reported by Kyriakou et al. [21], to date, where the authors used a mixture of vanadium (oxy)nitride and iron as cathode material for the electrochemical synthesis of ammonia. While the performance of this material was assessed in terms of ammonia formation and faradaic efficiency, limited attention has been given to the study of their fabrication and electrochemical behavior.

Therefore, we study the use of niobium (oxy)nitride ($NbN_xO_y$) as a potential electrode component for PCMRs. Differing from previous literature on a single (oxy)nitride phase electrode, in our work, a composite made with a perovskite proton-conducting ceramic is proposed. The current work underscores for the first time the chemical compatibility between the $NbN_xO_y$ phase and the ceramic electrolyte, while also providing a method for electrode fabrication, followed by a detailed mechanistic study of the electrode mechanism in reducing atmospheres, using a symmetrical cell arrangement. The mechanism is tentatively explained for both oxidation and reduction reactions aiming to understand the potential application of the novel composite electrode for both hydrogenation/de-hydrogenation of ammonia.

## 2. Experimental

### 2.1. Powder synthesis

$BaCe_{0.7}Zr_{0.1}Y_{0.2}O_{3-\delta}$ (BCZY712) electrolyte powder was synthesized by an acetate-$H_2O_2$ combustion method, as reported in detail previously [23]. Niobium (oxy)nitride ($NbN_xO_y$) material was produced by nitridation of niobium pentoxide ($Nb_2O_5$, Sigma-Aldrich) at 700 °C for 12 h in a tubular furnace under a flowing $NH_3$ atmosphere (Air Liquide, purity > 99.8 %). Phase purity was analyzed by X-ray diffraction (XRD) analysis using a *Rigaku SmartLabSe* diffractometer, 2θ = 20–80°, with a scan rate 3° $min^{-1}$ (Cu-Kα radiation, wavelength of 1.5406 Å, 40 kV, 30 mA).

The chemical compatibility between the $NbN_xO_y$ and the BCZY712 materials was assessed by mixing powders of both compositions in a proportion of 50:50 wt% ratio, followed by pelletizing (uniaxial pressing) and calcination at 850 °C in a nominally dry ($p_{H2O} \sim 10^{-5}$ atm) 10 % $H_2/N_2$ atmosphere (formic gas, Air Liquide, purity > 99.8 %) for 12 h. The calcined mixture was then evaluated by XRD to analyze phase composition.

### 2.2. Stability in different atmospheres

The phase stability of the $NbN_xO_y$ powders was assessed by thermogravimetric experiments (TG) in nominally dry $N_2$ (Air Liquide, purity > 99.8 %), 10 % $H_2/N_2$ (formic gas, Air Liquide, purity > 99.8 %), and 2 % $H_2/N_2$, *i.e.*, 10 % $H_2/N_2$-$N_2$ mixtures, at 900 °C, with a heating rate of 3 °C $min^{-1}$ and dwell time of 1 h.

### 2.3. Symmetrical cell fabrication

A symmetrical cell made with the BCZY712-$NbN_xO_y$|BCZY712|BCZY712-$NbN_xO_y$ configuration was prepared. A dense BCZY712 electrolyte substrate was fabricated by applying isostatic pressure (350 MPa for 15 min) and sintering at 1550 °C for 10 h. BCZY712-$NbN_xO_y$ electrode slurries were prepared by carefully mixing 40 vol% of the $NbN_xO_y$ and 60 vol% of the BCZY712 powders with terpineol and stearic acid in an agate mortar. After that, two layers were symmetrically screen-printed on the surfaces of the densified BCZY712 substrate. The final BCZY712-$NbN_xO_y$|BCZY712|BCZY712-$NbN_xO_y$ symmetrical assembly was heated in a dry reducing atmosphere (10 % $H_2/N_2$) at 500 °C for 2 h to evaporate organics, followed by sintering at 850 °C for 3 h.

The morphology and microstructure of the symmetrical cell were observed by scanning electron microscopy (SEM, *Hitachi SU-70*) coupled with Energy-dispersive X-ray spectroscopy (EDS, *Brucker Quantax 400 detector*) for analyzing the elemental mapping distribution.

### 2.4. Electrochemical characterization

Electrochemical studies were performed by electrochemical impedance spectroscopy (EIS) using an Electrochemie-Autolab PGSTAT302N frequency response analyzer in the frequency range 1 MHz–0.01 Hz with a signal amplitude of 50 mV.

Single atmospheres were composed of nominally dry 10 % $H_2/N_2$ (formic gas, Air Liquide, purity > 99.8 %), $NH_3$ (Air Liquide, purity > 99.8 %), and 75 % $H_2/N_2$, a mixture of 75 % of $H_2$ (Air Liquide, purity > 99.8 %) and 25 % of $N_2$ (Air Liquide, purity > 99.8 %) gases. Measurements were performed at 50 °C intervals, in the direction of decreasing temperature, in the temperature range of 750–500 °C. Variation of the hydrogen partial pressure ($p_{H2}$) was performed at 50 °C intervals in the direction of decreasing temperature, in the temperature range of 500–750 °C, by mixing nominally dry 10 % $H_2/N_2$ with $N_2$ mixtures until a minimum $p_{H2} = 0.1$ atm was achieved. These dry atmospheres, with values of $p_{H2O} \sim 10^{-5}$–$10^{-4}$ atm [12], were achieved using an SGT super clean gas moisture filter.

A complimentary measurement in wet conditions was also performed by a wetted 10 % $H_2/N_2$ formic gas that had been bubbled through KBr-saturated $H_2O$, allowing to achieve a $p_{H2O} \sim 10^{-2}$ atm. The relative humidity was determined using a temperature and humidity sensor (JUMO, 907023). The gases were applied to the measurement jig with a maximum total flowrate of 50 mL $min^{-1}$, supplied by *Bronkhorst* Thermal Mass flow Controllers (EL Flow). Oxygen sensor values were measured using a YSZ (*Friatec*) sensor inserted in the sample jig.

The dwell time at each temperature before each measurement was 1 h, and stability was confirmed by performing repeated impedance measurements after an additional 1 h. The obtained impedance spectra were fitted using a non-linear least squares fitting (equivalent circuits) using the software ZView© (Scribner Associates), allowing to calculate the resistance and the capacitance values associated with each individual process.

## 3. Results and discussion

### 3.1. Phase purity and chemical compatibility analysis

Chemical compatibility is an important feature to ensure the higher lifetime and performance of cell components [24]. In this regard, by using X-ray diffraction (XRD), the chemical reactivity between the $NbN_xO_y$ compound and BCZY712 electrolyte composition in 10%$H_2/N_2$ was evaluated. Fig. 1a shows the diffractogram obtained for the synthesized BCZY712 electrolyte composition, where a pure phase was obtained, being indexed to the expected orthorhombic symmetry [25,26]. Moreover, both materials, $NbN_xO_y$ and BCZY712, do not show inter-reactivity at 850 °C, for 12 h, as verified in Fig. 1b. Conversely, at 950 °C, both phases reacted, leading to the formation of a $BaNb_2O_6$ phase, which was reported to be a solid solution within the BaO-$Nb_2O_5$ system [27]. Thus, the temperature of 850 °C was selected to perform the sintering of electrodes used in the subsequent sections.

### 3.2. Stability of the $NbN_xO_y$ phase

To evaluate the stability of the $NbN_xO_y$ phase, thermogravimetric (TG) measurements were made in conditions near the predicted stability limit of this material: pure $N_2$ and 2 % $H_2/N_2$, from RT to 900 °C, as shown in Fig. 2.a. After measurements, powders were analyzed by XRD to identify possible phase decomposition (Fig. 2.b) while *Rietveld* analysis was used to monitor potential lattice parameter changes.

In a pure $N_2$ atmosphere, $NbN_xO_y$ shows a total weight gain of ~10 %, which initiates at $T \sim 100$ °C (Fig. 2.a), due to the partial oxidation and decomposition of niobium (oxy)nitride into niobium pentaoxide ($Nb_2O_5$) (Fig. 2.b), according to,

$$NbO_xN_y(s) + \left(\frac{2.5-x}{2}\right)O_2(g) \rightarrow \frac{1}{2}Nb_2O_5(s) + \left(\frac{y}{2}\right)N_2(g) \quad (1)$$

In contrast, in a 2 % $H_2/N_2$ atmosphere, the weight variation remains effectively constant (Fig. 2.a). From the XRD pattern in Fig. 2.b, it is possible to observe that the $NbN_xO_y$ phase maintains the structural integrity of its rock-salt structure, albeit with a slight peak shift towards higher 2θ angles, corresponding to a lattice parameter change of 4.3116 (3) to 4.3377(2), which may be related to a slight increase in the N/O ratio of the anionic sublattice [28].

### 3.3. Microstructure of the sintered film and thermal expansion coefficient

Fig. 3 depicts the thermal expansion coefficient (TEC) of the $NbN_xO_y$ material measured in the temperature range of 200–800 °C, upon heating. A constant TEC value of $8.24 \times 10^{-6}$ °$C^{-1}$ was determined in the whole measured temperature range. Conversely, the BCZY712 material (Fig. 3) exhibits a change in slope at around 600 °C, which is potentially related to the typical dehydration of this material at high temperatures, as expected for this type of proton-conducting perovskites [29,30]. In this regard, the recent review from Løken et al. [31] ascribed this behavior to the loss of protons from the perovskite structure, resulting in a decrease in apparent TEC with increasing temperature, as observed, while the hydrated BCZY712 material should possess a constant TEC value of around $12 \times 10^{-6}$ °$C^{-1}$, in agreement to the current results at lower temperatures [31]. Therefore, within the targeted temperature range of operation for these materials (400–600 °C), the similarity of the measured TEC values for these two materials, highlights another potential advantage of using $NbN_xO_y$ as an electrode material, in comparison to that of metallic Ni-BCZY cermets which show a much higher TEC of around 17–18 $\times 10^{-6}$ °$C^{-1}$ [32,33].

Fig. 4a shows the microstructure of the sintered electrode film made of the BCZY712-$NbN_xO_y$ film produced by the screen-printing method. The electrode film, with a thickness of ~20 μm, shows a porous microstructure (as shown in the magnification), also presenting an average grain size at the submicron level. The porosity shown to be present can be suggested to be fundamental to facilitate good gas phase diffusion to the TPB [34]. Also, good adhesion between the cathode and

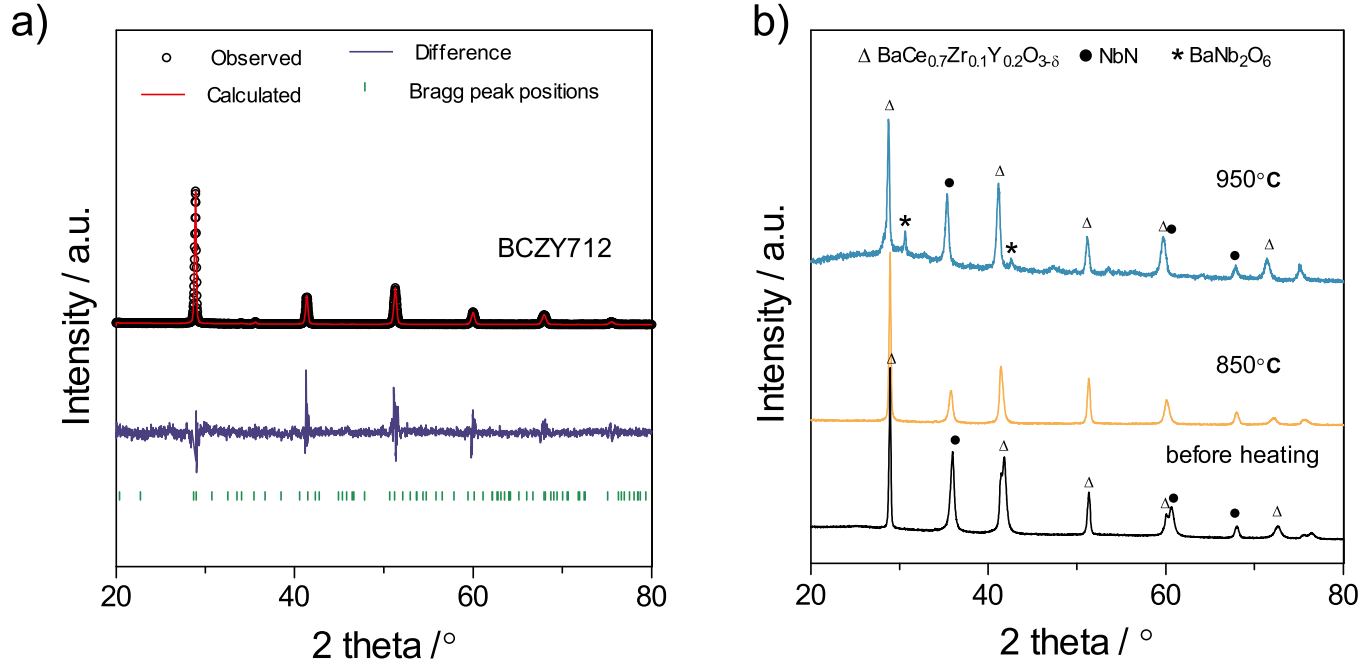


**Fig. 1.** X-ray diffraction (XRD) patterns of a) 40 vol% of $NbN_xO_y$-BCY10 composite before and after exposure at 850 °C, 750 °C and 650 °C in 10 % $H_2/N_2$ b) $Ba_{1-x}Ce_{0.9}Y_{0.1}O_{3-\delta}$ powders c) 40 vol% of $NbN_xO_y$-$Ba_{1-x}Ce_{0.9}Y_{0.1}O_{3-\delta}$ powders after heating at 850 °C in 10 % $H_2/N_2$ for 12 h.

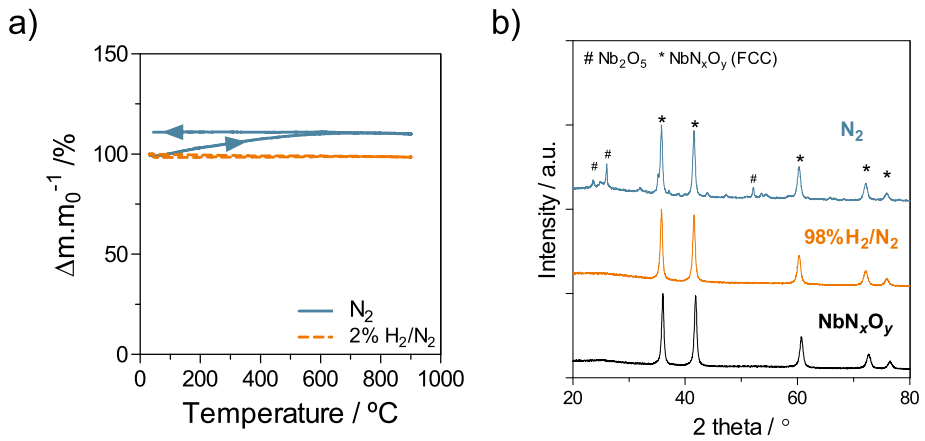


**Fig. 2.** a) Thermogravimetric (TG) analyses made on $NbN_xO_y$ powders in different atmospheres in the temperature range RT to 900 °C; b) X-ray diffraction (XRD) patterns of the resultant powders after treatment compared to the as-synthesized $NbN_xO_y$ powder.

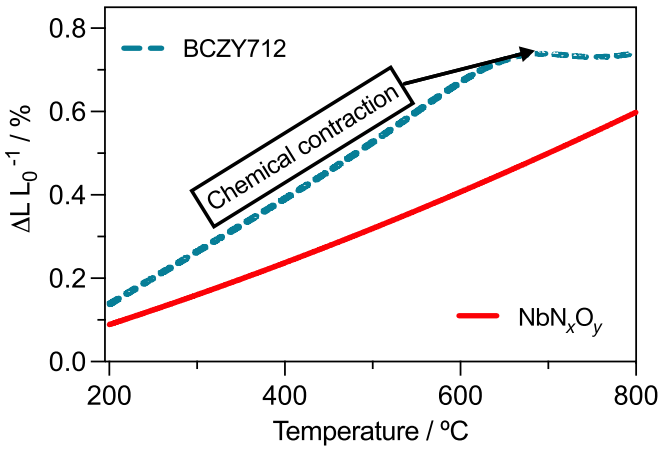


**Fig. 3.** Linear expansion (%) obtained for the $NbN_xO_y$ and the BCZY712 sintered bars, measured in a nominally dry 10 % $H_2/N_2$ atmosphere in heating mode (200–800 °C).

electrolyte interface can be noted, potentially benefitted by the similar values for the thermal expansion coefficient determined for the BCZY712 and $NbN_xO_y$ samples (Fig. 3). Moreover, from the Energy-dispersive Spectroscopy (EDS) analysis, a coherent mixing between both phases was achieved, potentially resulting in a good percolation of both phases [34–36].

### 3.4. Electrochemical behavior of the BCZY712-$NbN_xO_y$ electrode

Electrochemical Impedance Spectroscopy (EIS) was performed using a symmetrical cell made with the BCZY712-$NbN_xO_y$|BCZY712|BCZY712-$NbN_xO_y$ configuration, which was prepared to study the electrochemical characteristics of the BCZY712-$NbN_xO_y$ electrode. Measurements were made in the temperature range of 500 °C–750 °C in different atmospheres. Fig. 5a shows example impedance spectra obtained at 750 °C in 75 % $H_2/N_2$, 2 % $H_2/N_2$ and in pure $NH_3$. The impedance spectra are similar in shape among all samples, being composed of two semicircles at high- and middle-frequency, with resistance terms denominated $R_{HF}$ and $R_{MF}$, respectively. Additionally, a low-frequency electrode tail, can also be observed, although it cannot be completely resolved within the frequency range of the equipment measurement window. This low-frequency tail is noted to disappear with decreasing temperature (results not shown).

To fit the impedance data, an equivalent circuit, inset in Fig. 5.b, consisting of an inductance ($L$) in series with a resistor ($R_{ohm}$), which represents the cell ohmic resistance, two distributed $R||Q$ elements and a *Warburg* element was used. The resistance ($R$), the pseudo-capacitance ($Q$), and the parameter $n$ are the values extracted for each semicircle applying the fitting model. The polarization resistance values obtained were multiplied by the electrode area and divided by a factor of 2 due to the symmetrical cell configuration. By using the following equation, it is

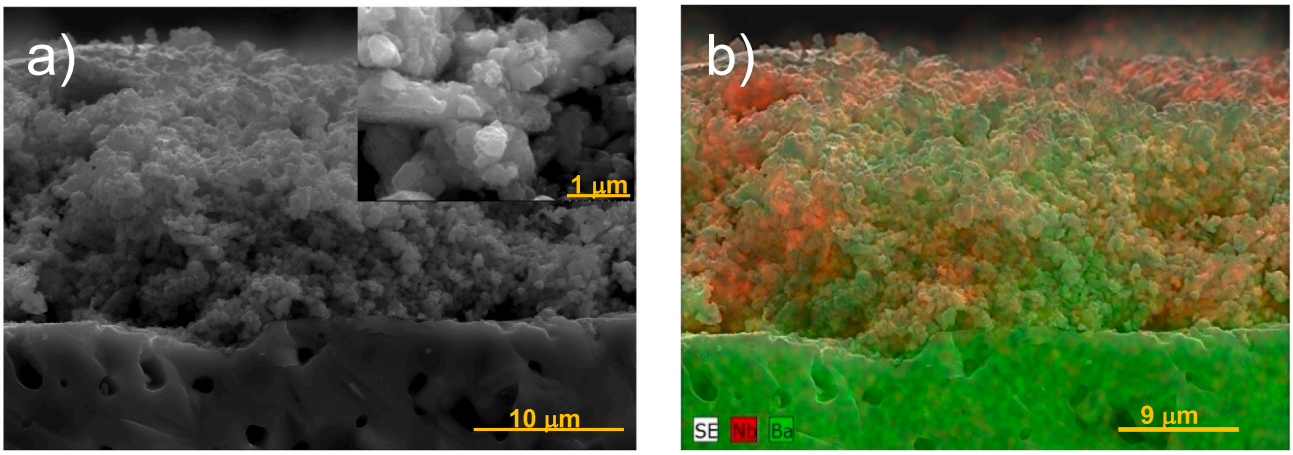


**Fig. 4.** a) Cross-section microstructure of the symmetrical cell made with the BCZY712-$NbN_xO_y$|BCZY712|BCZY712-$NbN_xO_y$ configuration (40 vol% of the $NbN_xO_y$ phase) (the inset presents a detailed view with a higher magnification); b) corresponding energy-dispersive spectroscopy (EDS) mapping.

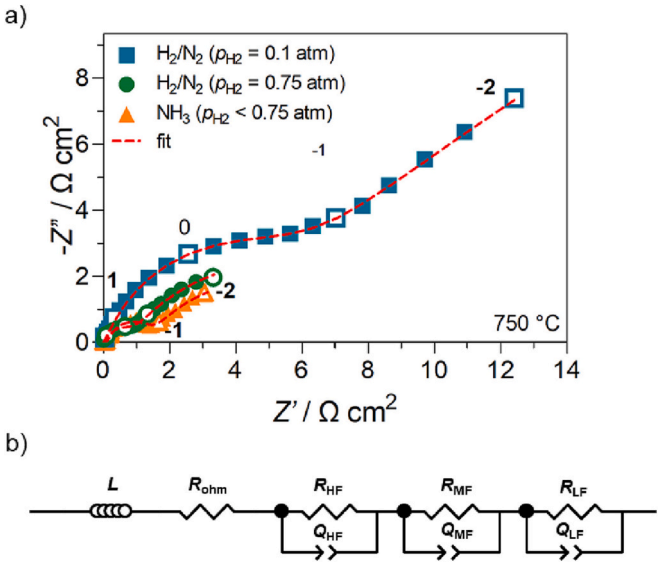


**Fig. 5.** a) Impedance spectra of the symmetrical cell with BCZY712-$NbN_xO_y$ electrode measured in dry 10 % $H_2/N_2$, 75 % $H_2/N_2$ and $NH_3$ at 750 °C (the numbers indicate the decades ($log_{10}$) of the measuring frequencies; the high-frequency intersect was removed for better visualization). b) Equivalent circuit used to fit the impedance spectra.

possible to calculate the true capacitance:

$$C = R^{(1-n)/n}Q^{(1/n)} \quad (2)$$

From the first inspection of Fig. 6, it is possible to observe a less resistive behavior with the increase of %$H_2$ present in the atmosphere. Additionally, it is possible to observe that $NbN_xO_y$ shows a lower total resistance in 75 % $H_2/N_2$ than in pure $NH_3$.

The BCZY712-$NbN_xO_y$ electrode shows a value with the order of magnitude in the range of $10^{-6}$–$10^{-5}$ F $cm^{-2}$ and $10^{-3}$–$10^{-2}$ F $cm^{-2}$ associated with the semicircle at high- and middle-frequency, respectively. From a comparison of these calculated values with typical values of other comparable electrodes in the literature, $R_{HF}$ can be most likely associated with interfacial transfer phenomena, while $R_{MF}$ can be associated with surface reactions occurring at the triple phase boundaries (TPBs) [35,37,38,40].

Fig. 6 shows the hydrogen partial pressure ($p_{H2}$) dependence of the high-frequency polarization resistance ($R_{HF}$) of the BCZY712-$NbN_xO_y$ electrode obtained in nominal mixtures of 10 % $H_2/N_2$ and $N_2$ gases, in the temperature range 500–600 °C. Data at higher temperatures were not included as the $R_{HF}$ term gradually decreases, disappearing at high temperatures ($T \geq 650$ °C). Moreover, $R_{HF}$ is shown to have a weak dependence on the $p_{H2}$ level. This behavior resembles the typical interfacial transfer processes occurring at the electrode-electrolyte interface, corroborating the very low capacitance values estimated for this term ($10^{-6}$–$10^{-5}$ F $cm^{-2}$) [38,41]. Due to the proton-conducting nature of the BCZY712 phase, the formation of protonic charge carriers could be expected [43,44],

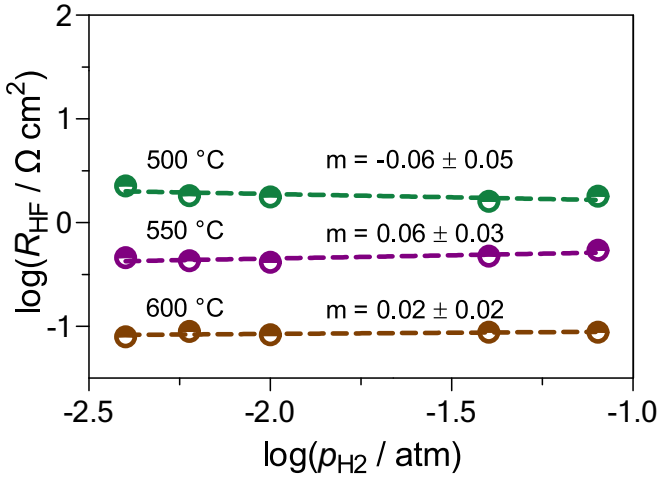


**Fig. 6.** The hydrogen partial pressure ($p_{H2}$) dependence of the high-frequency polarization resistance ($R_{HF}$) of the BCZY712-$NbN_xO_y$ electrode obtained in nominal mixtures of 10 % $H_2/N_2$ and $N_2$ atmospheres in the temperature range 500–600 °C.

$$H_2O + V_O^{\cdot\cdot} + O_O^x \leftrightarrow 2OH_O^{\cdot} \quad (3)$$

Thus, the following equation could characterize the $R_{HF}$ processes:

$$OH^{\cdot}_{O,electrode} + O^x_{O,electrolyte} \leftrightarrow OH^{\cdot}_{O,electrolyte} + O^x_{O,electrode} \quad (4)$$

However, in nominally dry reducing conditions, it is well-known that, above 400 °C, a gradual transition is typically observed from proton to oxygen-ion conductivity [11,12], thus, the formation of competing oxygen-ion vacancies ($V_O^{\cdot\cdot}$) cannot be excluded,

$$V^{\cdot\cdot}_{O,electrode} + O^x_{O,electrolyte} \leftrightarrow V^{\cdot\cdot}_{O,electrolyte} + O^x_{O,electrode} \quad (5)$$

In this respect, the $E_a$ values registered for $R_{HF}$ (varying in the 1.24 eV–1.79 eV for the different atmospheres, Table 1), measured across the temperature range 750–500 °C, are much higher than that expected for pure protonic conductivity, *i.e.*, typically around 0.50 eV [14], suggesting that oxygen-ion partial conductivity may be relevant, where a value of 1.6 eV was previously reported in reducing atmospheres [12]. In addition, no n-type electronic conductivity is expected due to the very low Ce reducibility in the perovskite under these measurement conditions [12]. This behavior was also reported for other doped-barium cerates, where only under severe reducing conditions and very high temperatures there is an appreciable alteration of the oxygen-vacancy concentration [45,46], with a subsequent impact in the n-type electronic transport [12].

Fig. 7 shows the middle-frequency polarization resistance ($R_{MF}$) as a function of the temperature of the BCZY712-$NbN_xO_y$ electrode for $NH_3$, 75 % $H_2N_2$ and 10 % $H_2/N_2$ atmospheres. As one can see, the $R_{MF}$ contribution decreases by nearly one order of magnitude upon increasing the $p_{H2}$ from 0.1 atm to 0.75 atm, across the complete temperature range.

Nonetheless, a remarkable behavior is shown in the case of the $NH_3$ atmosphere, where the $R_{MF}$ term shows a much higher $E_a$ value, than that of the $H_2/N_2$ atmospheres. In this regard, incomplete ammonia decomposition must be considered, as also shown experimentally by Miyazaki et al. [47] for Ni-based cermet anodes, under a pure $NH_3$ atmosphere, given by

$$2NH_3(g) \rightarrow 3H_2(g) + N_2(g) \quad (6)$$

This behavior results in a sharp increase in the $E_a$ value to 1.81 eV, in comparison to the $E_a$ values determined for both 75 % $H_2/N_2$ (1.31 eV) and 10 % $H_2/N_2$ (1.24 eV) atmospheres (Table 1), thus, suggesting that

**Table 1**
Activation energy ($E_a$) values obtained for the polarization resistances under different atmospheres.

| Term | Atmosphere | Activation energy ($E_a$)/eV |
|---|---|---|
| $R_{HF}$ | $NH_3$ ($p_{H2}$ < 0.75 atm) | 1.24 |
| | Dry $H_2/N_2$ ($p_{H2}$ = 0.75 atm) | 1.74 |
| | Dry $H_2/N_2$ ($p_{H2}$ = 0.1 atm) | 1.44 |
| $R_{MF}$ | $NH_3$ ($p_{H2}$ < 0.75 atm) | 1.84 |
| | Dry $H_2/N_2$ ($p_{H2}$ = 0.75 atm) | 1.31 |
| | Dry $H_2/N_2$ ($p_{H2}$ = 0.1 atm) | 1.24 |
| $R_{LF}$ | Dry $H_2/N_2$ ($p_{H2}$ = 0.75 atm) | 0.22 |

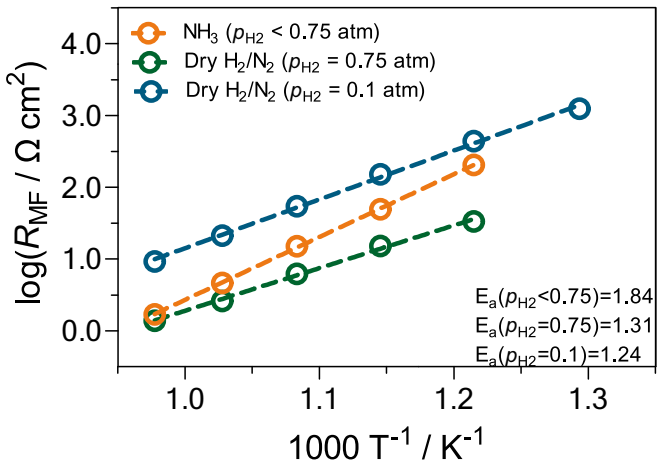


**Fig. 7.** The temperature dependence of the middle-frequency polarization resistance ($R_{MF}$) of the BCZY712-NbN$_x$O$_y$ electrode obtained in nominally dry $NH_3$, 75 % $H_2/N_2$, and 10 % $H_2/N_2$ atmospheres.

free $H_2$ fraction plays an important role on this term. Moreover, this result also highlights that NbN$_x$O$_y$ is not a good catalyst for $NH_3$ dissociation at low temperatures, due to the different behaviors of the middle-frequency polarization resistance ($R_{MF}$) observed under 75 % $H_2/N_2$ and $NH_3$ atmospheres; a potentially promising result for the potential use of this material for ammonia production. To further understand this $p_{H2}$ behavior of the composite electrode in further depth, Fig. 8 shows the dependence of $R_{MF}$ on $p_{H2}$, which is shown to have a strong negative power dependence, $m \sim -0.5$, for all measured temperatures.

The typical rate-limiting steps for $H_2$ reaction at the surface usually involve either dissociative adsorption (or also, $H_2$ desorption in the reverse reaction) [35,38],

$$H_2(g) \leftrightarrow H_{2,ads} \ (m = 0.5) \tag{7}$$

or oxidation reaction of hydrogen (or also, reduction of protons to hydrogen in the reverse reaction) [38].

$$H_{ads} \leftrightarrow H^+_{ads} + e^- \ (m = 0.25) \tag{8}$$

Based on the $m = 0.5$ dependence observed in Fig. 8, $R_{MF}$ can be best attributed to the adsorption/desorption of $H_2$ at the surface of the electrocatalyst, Eq. (7). Moreover, the larger resistance of $R_{MF}$ compared with $R_{HF}$ suggests that the former is the dominant rate limiting step for

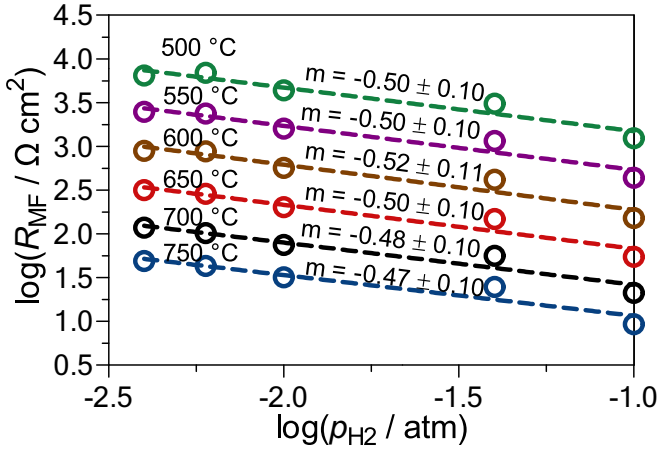


**Fig. 8.** The hydrogen partial pressure ($p_{H2}$) dependence of the middle-frequency polarization resistance ($R_{MF}$) of the BCZY712-NbN$_x$O$_y$ electrode obtained in nominal mixtures of 10 % $H_2/N_2$ and $N_2$ atmospheres in the temperature range 500–750 °C.

the BCZY712-NbN$_x$O$_y$ electrode [35,38].

Fig. 9a shows the temperature dependence of the low-frequency polarization resistance ($R_{LF}$). The analysis in the whole measured temperature range was not possible in pure $NH_3$ or in the 10 % $H_2/H_2$ atmospheres. Nonetheless, in the case of the 75 % $H_2/H_2$ atmosphere, the $R_{LF}$ term is clearly shown to have a low temperature dependence, $E_a$ = 0.22 eV (Table 1), as typically expected for gas-phase-related processes [48]. Moreover, the magnitude of the $R_{LF}$ term is also observed to be similar in both $NH_3$ and 75 % $H_2$ atmospheres, as shown in Fig. 9.b for the measurement temperature of 800 °C, while, in the 10 % $H_2/H_2$ atmosphere, $R_{LF}$ increases by almost one order of magnitude at this temperature, suggesting a negative dependence of $R_{LF}$ on the $p_{H2}$ level (Fig. 9b).

Based on previous reports on proton-conducting composite electrodes, the low-frequency polarization resistance ($R_{LF}$) to proton incorporation (or water release in the reverse reaction) may be ascribed to the following reactions [34,49–52],

$$H_2O_{ads} + V_O^{\cdot\cdot} \rightarrow O^x_{O,electrode} \leftrightarrow 2OH^{\cdot}_{O,electrode} \tag{9}$$

and/or water adsorption (or desorption in the reverse reaction),

$$H_2O(g) \leftrightarrow H_2O_{ads} \tag{10}$$

In this respect, Fig. 10 compares the impedance dispersions of the BCZY712-NbN$_x$O$_y$ electrode tested in both nominally dry ($p_{H2O} \sim 10^{-5}$ atm) and wet ($p_{H2O} \sim 10^{-2}$ atm) conditions at 750 °C. From this comparison, it can be immediately observed that the $R_{LF}$ process is only predominant in nominally dry conditions, while effectively disappearing in wet conditions. This strong dependence on the $p_{H2O}$ level suggests that the adsorbed water ($H_2O_{ads}$) may be involved in the process. The presence of the low-frequency electrode tail is characteristic of diffusion processes, possibly suggesting that the molecular gaseous water diffusion is rate limiting under dry conditions, being further impaired at lower $p_{H2}$ values (which are expected to result in slightly lower intrinsic $p_{H2O}$ values [12]), while, conversely, being promoted under the wet conditions. This concept may be further corroborated by the very high capacitance values estimated for this term (>1 F cm$^{-2}$), (characteristic of diffusion limited behavior) [34,49–52]. In contrast, both the $R_{HF}$ and $R_{MF}$ processes are shown to be effectively independent of the $p_{H2O}$ level. In wet conditions, therefore, the $R_{MF}$ process becomes predominant, in agreement with a previous work by Nasani et al. [35] made on Ni-BZY analogs and concurring with their suggested limiting electrode mechanisms described above.

To summarize the above information, a tentative global electrode mechanism for the 40 vol% BCZY712-NbN$_x$O$_y$ composite electrode will now be elaborated. In this respect, Fig. 11 illustrates the possible reaction steps described by the elementary steps of the polarization resistance that were determined in the previous sections. The reaction steps are provided in terms of both oxidation and reduction reactions. Hence, the mechanism for the electrochemical oxidation of gaseous $H_2$ involves three main steps, namely, i) proton incorporation/water release or adsorption/desorption of water, ii) gaseous hydrogen adsorption/desorption, and iii) interfacial transfer reaction of either protons or oxygen-ion vacancies. As shown in Fig. 11, the surface reactions can occur predominantly at the triple phase boundaries (TPBs) [55]. Finally, in the specific case of the ammonia formation reaction, further studies under applied cathodic polarization are necessary together with quantitative ammonia-formation techniques, such as gas chromatography, to provide further data for the interpretation of the electrode mechanism towards $NH_3$ synthesis.

## 4. Conclusions

The current work provides a systematical approach to processing, electrode fabrication, chemical stability, and electrochemical characterization of a new category of a composite electrode made of niobium

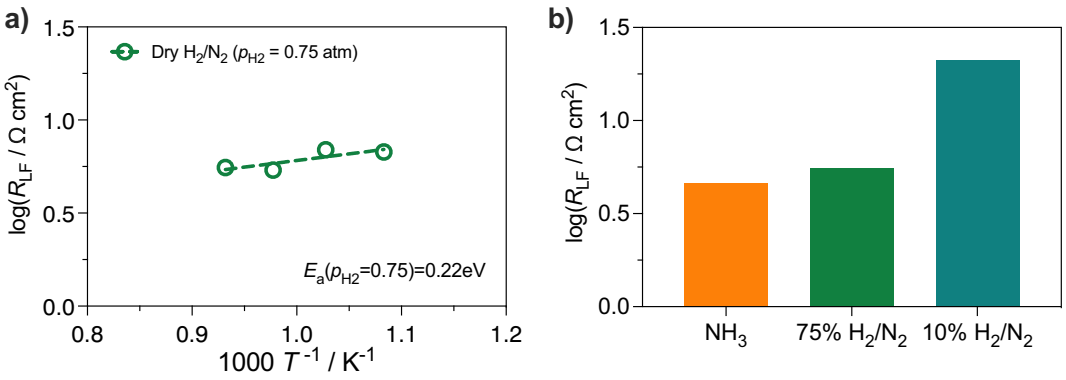


**Fig. 9.** The low-frequency polarization resistance ($R_{LF}$) of the BCZY712-$NbN_xO_y$ electrode obtained in nominally dry $NH_3$, 75 % $H_2/H_2$, and 10 % $H_2/H_2$ atmospheres: a) temperature dependence; b) comparison of $R_{LF}$ at 800 °C as a function of gas atmosphere.

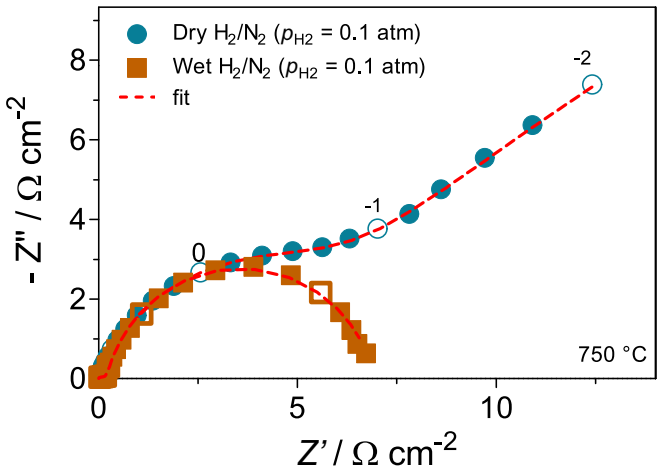


**Fig. 10.** Impedance spectrum of symmetrical cell with composite of 40 vol% BCZY712-$NbN_xO_y$ measured in dry 10 % $H_2/N_2$ ($p_{H2O} \sim 10^{-5}$ atm) and wet 10 % $H_2/N_2$ ($p_{H2O} \sim 10^{-2}$ atm) at 750 °C. The numbers indicate the decades ($\log_{10}$) of the measuring frequencies.

(oxy)nitride ($NbN_xO_y$) and a proton-conducting perovskite.

BCZY712 was shown to be chemically stable up to 850 °C, thus, facilitating the sintering process of the electrode film. Moreover, thermogravimetric experiments combined with X-ray diffraction after tests were also made to assess the thermal stability of the $NbN_xO_y$ material in both $N_2$ and 2 % $H_2/N_2$ atmospheres, revealing that $NbN_xO_y$ decomposes into parent oxides in $N_2$, while, conversely, retaining its phase purity in reducing conditions.

The polarization behavior of BCZY712-$NbN_xO_y$ composite electrode (40/60 vol%) compositions was evaluated by electrochemical impedance spectroscopy under different atmospheric conditions. The overall electrode mechanism was tentatively explained by three main steps, including, i) proton incorporation/water release or adsorption/desorption of water, ii) gaseous hydrogen adsorption/desorption, and iii) interfacial transfer reaction of either protons or oxygen-ion vacancies.

## CRediT authorship contribution statement

**Vanessa C.D. Graça:** Formal analysis, Investigation, Writing – original draft, Writing – review & editing. **Laura I.V. Holz:** Formal analysis, Investigation, Writing – original draft, Writing – review & editing. **Allan J.M. Araújo:** Formal analysis, Investigation, Writing – original draft, Writing – review & editing. **Francisco J.A. Loureiro:** Formal analysis, Investigation, Writing – original draft, Conceptualization, Methodology, Resources, Writing – review & editing, Supervision, Funding acquisition. **Duncan P. Fagg:** Conceptualization, Methodology, Formal analysis, Writing – original draft, Resources, Writing – review & editing, Supervision, Funding acquisition.

## Declaration of competing interest

The authors declare that they have no known competing financial interests or personal relationships that could have appeared to influence

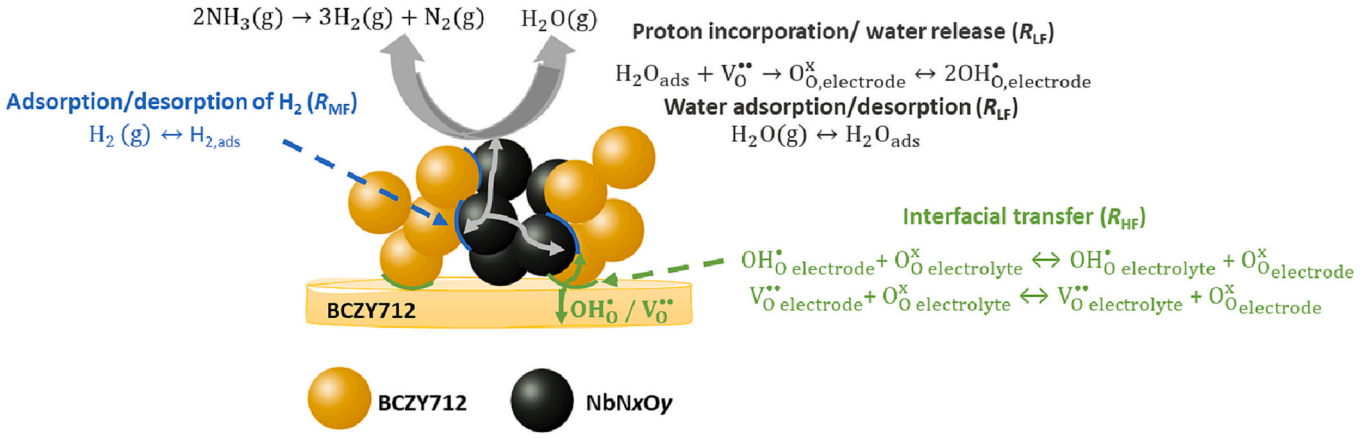


**Fig. 11.** Illustration of possible electrode reactions occurring when using $NbN_xO_y$-BCZY712 electrocatalysts in a $NH_3$- or $H_2$-based atmosphere in nominally dry reducing conditions. The overall electrode mechanism was tentatively explained by three main steps, including, i) proton incorporation/water release or adsorption/desorption of water, ii) gaseous hydrogen adsorption/desorption, and iii) interfacial transfer reaction of either protons or oxygen-ion vacancies.

the work reported in this paper.

## Data availability

Data will be made available on request.

## Acknowledgments

Vanessa C. D. Graça and Laura I. V. Holz are grateful to the Fundação para a Ciência e Tecnologia (FCT), for their Ph.D. grants, respectively, SFRH/BD/130218/2017 and PD/BDE/142837/2018. Francisco J. A. Loureiro is thankful for the Investigator Grant CEECIND/02797/2020. The authors also acknowledge the projects, 2022.02498.PTDC, 2022.09319.PTDC, PTDC/CTM-CTM/2156/2020, PTDC/QUI-ELT/3681/2020, POCI-01-0247-FEDER-039926, UIDB/00481/2020 and UIDP/00481/2020 from FCT, and CENTRO-01-0145-FEDER-181241 and CENTRO-01-0145-FEDER-022083 from Centro Portugal Regional Operational Programme (Centro2020), under the PORTUGAL 2020 Partnership Agreement, through the European Regional Development Fund (ERDF).

## Appendix A. Supplementary data

Supplementary data to this article can be found online at https://doi.org/10.1016/j.est.2023.107769.

## References

[1] C. Zamfirescu, I. Dincer, Using ammonia as a sustainable fuel, J. Power Sources 185 (2008) 459–465, https://doi.org/10.1016/j.jpowsour.2008.02.097.
[2] Z. Wan, Y. Tao, J. Shao, Y. Zhang, H. You, Ammonia as an effective hydrogen carrier and a clean fuel for solid oxide fuel cells, Energy Convers. Manag. 228 (2021) 113729, https://doi.org/10.1016/J.ENCONMAN.2020.113729.
[3] P. Dimitriou, R. Javaid, A review of ammonia as a compression ignition engine fuel, Int. J. Hydrog. Energy 45 (2020) 7098–7118, https://doi.org/10.1016/j.ijhydene.2019.12.209.
[4] L. Zhu, C. Cadigan, C. Duan, J. Huang, L. Bian, L. Le, C.H. Hernandez, V. Avance, R. O'Hayre, N.P. Sullivan, Ammonia-fed reversible protonic ceramic fuel cells with Ru-based catalyst, Commun. Chem. 1 (4) (2021) 1–10, https://doi.org/10.1038/s42004-021-00559-2 (2021 4).
[5] E.C. Blanco, A. Sánchez, M. Martín, P. Vega, Methanol and ammonia as emerging green fuels: evaluation of a new power generation paradigm, Renew. Sust. Energ. Rev. 175 (2023) 113195, https://doi.org/10.1016/j.rser.2023.113195.
[6] A.G. Olabi, M.A. Abdelkareem, M. Al-Murisi, N. Shehata, A.H. Alami, A. Radwan, T. Wilberforce, K.-J. Chae, E.T. Sayed, Recent progress in Green Ammonia: production, applications, assessment; barriers, and its role in achieving the sustainable development goals, Energy Convers. Manag. 277 (2023) 116594, https://doi.org/10.1016/j.enconman.2022.116594.
[7] H. Zhang, Y. Zhou, K. Pei, Y. Pan, K. Xu, Y. Ding, B. Zhao, K. Sasaki, Y. Choi, Y. Chen, M. Liu, An efficient and durable anode for ammonia protonic ceramic fuel cells, Energy Environ. Sci. 15 (2022) 287–295, https://doi.org/10.1039/D1EE02158C.
[8] F. He, Q. Gao, Z. Liu, M. Yang, R. Ran, G. Yang, W. Wang, W. Zhou, Z. Shao, A new Pd doped proton conducting perovskite oxide with multiple functionalities for efficient and stable power generation from Ammonia at reduced temperatures, Adv. Energy Mater. 11 (2021) 2003916, https://doi.org/10.1002/AENM.202003916.
[9] V. Kyriakou, I. Garagounis, E. Vasileiou, A. Vourros, M. Stoukides, Progress in the electrochemical synthesis of ammonia, Catal. Today 286 (2017) 2–13, https://doi.org/10.1016/j.cattod.2016.06.014.
[10] I. Garagounis, A. Vourros, D. Stoukides, D. Dasopoulos, M. Stoukides, Electrochemical synthesis of ammonia: recent efforts and future outlook, Membranes 9 (2019) 112 (9 (2019) 112), https://doi.org/10.3390/MEMBRANES9090112.
[11] F.J.A. Loureiro, D. Ramasamy, A.F.G. Ribeiro, A. Mendes, D.P. Fagg, Underscoring the transport properties of yttrium-doped barium cerate in nominally dry oxidising conditions, Electrochim. Acta 334 (2020), https://doi.org/10.1016/j.electacta.2020.135625.
[12] F.J.A. Loureiro, D. Pérez-Coll, V.C.D. Graça, S.M. Mikhalev, A.F.G. Ribeiro, A. Mendes, D.P. Fagg, Proton conductivity in yttrium-doped barium cerate under nominally dry reducing conditions for application in chemical synthesis, J Mater Chem A Mater 7 (2019) 18135–18142, https://doi.org/10.1039/C9TA04584H.
[13] V.C.D. Graça, F.J.A. Loureiro, L.I.V. Holz, S.M. Mikhalev, D.P. Fagg, Assessment of the electrical properties and chemical stabilities of BaCe0.9Y0.1O3−δ and BaCe0.7Zr0.1Y0.2O3−δ proton ceramic electrolytes at low temperatures, 300 to 600°C, Int. J. Energy Res. (2022), https://doi.org/10.1002/er.8746 (n/a).
[14] F.J.A. Loureiro, Z. Shakel, V.C.D. Graça, D.P. Fagg, Effect of humidification on the grain boundary conductivity and space-charge effects in yttrium-doped barium cerate, Int. J. Hydrog. Energy 46 (2021) 23828–23838, https://doi.org/10.1016/J.IJHYDENE.2021.04.175.
[15] M. Hashinokuchi, M. Zhang, T. Doi, M. Inaba, Enhancement of anode activity and stability by Cr addition at Ni/Sm-doped CeO2 cermet anodes in NH3-fueled solid oxide fuel cells, Solid State Ionics 319 (2018) 180–185, https://doi.org/10.1016/j.ssi.2018.02.015.
[16] A.-M. Alexander, J.S.J. Hargreaves, C. Mitchell, The reduction of various nitrides under hydrogen: Ni3N, Cu3N, Zn3N2 and Ta3N5, Top. Catal. 55 (2012) 1046–1053, https://doi.org/10.1007/s11244-012-9890-3.
[17] B. Stoeckl, V. Subotić, M. Preininger, M. Schwaiger, N. Evic, H. Schroettner, C. Hochenauer, Characterization and performance evaluation of ammonia as fuel for solid oxide fuel cells with Ni/YSZ anodes, Electrochim. Acta 298 (2019) 874–883, https://doi.org/10.1016/j.electacta.2018.12.065.
[18] V.C.D. Graça, F.J.A. Loureiro, L.I.V. Holz, S.M. Mikhalev, A.J.M. Araújo, D.P. Fagg, in: M.R. Cesario, D.A.B.T.-H.C. de Macedo (Eds.), Chapter 18 - Electrochemical Ammonia Synthesis: Mechanism, Recent Developments, and Challenges in Catalyst Design, Elsevier, 2022, pp. 497–514, https://doi.org/10.1016/B978-0-323-85612-6.00018-8.
[19] Y. Abghoui, A.L. Garden, V.F. Hlynsson, S. Björgvinsdóttir, H. Ólafsdóttir, E. Skúlason, Enabling electrochemical reduction of nitrogen to ammonia at ambient conditions through rational catalyst design, Phys. Chem. Chem. Phys. 17 (2015) 4909–4918, https://doi.org/10.1039/c4cp04838e.
[20] Y. Abghoui, E. Skúlason, Onset potentials for different reaction mechanisms of nitrogen activation to ammonia on transition metal nitride electro-catalysts, Catal. Today 286 (2017) 69–77, https://doi.org/10.1016/j.cattod.2016.11.047.
[21] V. Kyriakou, I. Garagounis, A. Vourros, E. Vasileiou, M. Stoukides, An electrochemical Haber-Bosch process, Joule. 4 (2020) 142–158, https://doi.org/10.1016/j.joule.2019.10.006.
[22] J. Díez-Ramírez, V. Kyriakou, I. Garagounis, A. Vourros, E. Vasileiou, P. Sánchez, F. Dorado, M. Stoukides, Enhancement of Ammonia synthesis on a Co3Mo3N-Ag electrocatalyst in a K-βAl2O3 solid electrolyte cell, ACS Sustain. Chem. Eng. 5 (2017) 8844–8851, https://doi.org/10.1021/acssuschemeng.7b01618.
[23] N. Narendar, G.C. Mather, P.A.N. Dias, D.P. Fagg, The importance of phase purity in Ni–BaZr0.85Y0.15O3−δ cermet anodes – novel nitrate-free combustion route and electrochemical study, RSC Adv. 3 (2012) 859–869, https://doi.org/10.1039/C2RA22301E.
[24] A.V. Kasyanova, L.R. Tarutina, A.O. Rudenko, J.G. Lyagaeva, D.A. Medvedev, Ba(Ce,Zr)O 3 -based electrodes for protonic ceramic electrochemical cells: towards highly compatible functionality and triple-conducting behaviour, Russ. Chem. Rev. 89 (2020) 667–692, https://doi.org/10.1070/RCR4928.
[25] N. Nasani, D.P. Fagg, Novel nitrate-free acetate-H2O2 combustion synthesis, in: J. M. Grier (Ed.), Combustion: Types of Reactions, Fundamental Processes and Advanced Technologies, Nova Publishers, 2014, pp. 245–267.
[26] J. Dailly, G. Taillades, M. Ancelin, P. Pers, M. Marrony, High performing BaCe0.8Zr0.1Y0.1O3-δ-Sm0.5Sr0.5CoO3-δ based protonic ceramic fuel cell, J. Power Sources 361 (2017) 221–226, https://doi.org/10.1016/J.JPOWSOUR.2017.06.089.
[27] R.S. Roth, J.L. Waring, Phase equilibrium relations in the binary system barium oxide-niobium pentoxide, J. Res. Natl. Bur. Stand. A. Phys. Chem. 65A (1961) 337–344, https://doi.org/10.6028/jres.065a.036.
[28] L.I.V. Holz, V.C.D. Graça, F.J.A. Loureiro, S.M. Mikhalev, D. Mendes, A. Mendes, D. P. Fagg, Tailoring the anion stoichiometry and oxidation kinetics of vanadium (oxy)nitride by the control of ammonolysis conditions, J Mater Chem C Mater 10 (2022) 5608–5620, https://doi.org/10.1039/D2TC00545J.
[29] D. Han, K. Goto, M. Majima, T. Uda, Proton conductive BaZr0.8-xCexY0.2O3-δ: influence of NiO sintering additive on crystal structure, hydration behavior, and conduction properties, ChemSusChem. 14 (2021) 614–623, https://doi.org/10.1002/CSSC.202002369.
[30] D. Han, X. Liu, S. Bjørheim, T. Uda, D. Han, T. Uda, X. Liu, T.S. Bjørheim, Yttrium-doped barium zirconate-cerate solid solution as proton conducting electrolyte: why higher cerium concentration leads to better performance for fuel cells and electrolysis cells, Adv. Energy Mater. 11 (2021) 2003149, https://doi.org/10.1002/AENM.202003149.
[31] A. Løken, S. Ricote, S. Wachowski, Thermal and chemical expansion in proton ceramic electrolytes and compatible electrodes, Crystals 8 (2018), https://doi.org/10.3390/cryst8090365.
[32] M. Mori, T. Yamamoto, H. Itoh, H. Inaba, H. Tagawa, Thermal expansion of nickel-zirconia anodes in solid oxide fuel cells during fabrication and operation, J. Electrochem. Soc. 145 (1998) 1374–1381, https://doi.org/10.1149/1.1838468/XML.
[33] T.M.M. Heenan, J.B. Robinson, X. Lu, B. Tjaden, A. Cervellino, J.J. Bailey, D.J. L. Brett, P.R. Shearing, Understanding the thermo-mechanical behaviour of solid oxide fuel cell anodes using synchrotron X-ray diffraction, Solid State Ionics 314 (2018) 156–164, https://doi.org/10.1016/J.SSI.2017.10.025.
[34] F.J.A. Loureiro, D. Ramasamy, V.C.D. Graça, L.I.V. Holz, S.M. Mikhalev, D.P. Fagg, Analysis of La4Ni3O10±δ-BaCe0.9Y0.1O3-δ composite cathodes for proton ceramic fuel cells, Appl. Sci. 11 (2021) 3407 (11 (2021) 3407), https://doi.org/10.3390/APP11083407.
[35] N. Nasani, D. Ramasamy, A.D. Brandão, A.A. Yaremchenko, D.P. Fagg, The impact of porosity, pH2 and pH2O on the polarisation resistance of Ni–BaZr0.85Y0.15O3−δ cermet anodes for Protonic Ceramic Fuel Cells (PCFCs), Int. J. Hydrog. Energy 39 (2014) 21231–21241, https://doi.org/10.1016/J.IJHYDENE.2014.10.093.

[36] A.J.M. Araújo, F.J.A. Loureiro, J.P.F. Grilo, D.A. Macedo, C.A. Paskocimas, D. P. Fagg, A high-performance oxygen electrode for solid oxide cells: compositional optimisation of barium cobaltite-based composites, J. Alloys Compd. 906 (2022) 164382, https://doi.org/10.1016/J.JALLCOM.2022.164382.

[37] F. He, T. Wu, R. Peng, C. Xia, Cathode reaction models and performance analysis of Sm0.5Sr0.5CoO3−δ–BaCe0.8Sm0.2O3−δ composite cathode for solid oxide fuel cells with proton conducting electrolyte, J. Power Sources 194 (2009) 263–268, https://doi.org/10.1016/J.JPOWSOUR.2009.04.053.

[38] L. Bi, E. Fabbri, Z. Sun, E. Traversa, BaZr0.8Y0.2O3−δ-NiO composite anodic powders for proton-conducting SOFCs prepared by a combustion method, J. Electrochem. Soc. 158 (2011), B797, https://doi.org/10.1149/1.3591040/XML.

[40] P. Pers, V. Mao, M. Taillades, G. Taillades, Electrochemical behavior and performances of Ni-BaZr0·1Ce0·7Y0.1Yb0.1O3−δ cermet anodes for protonic ceramic fuel cell, Int. J. Hydrog. Energy 43 (2018) 2402–2409, https://doi.org/10.1016/J.IJHYDENE.2017.12.024.

[41] E. Fabbri, S. Licoccia, E. Traversa, E.D. Wachsman, Composite cathodes for proton conducting electrolytes, Fuel Cells 9 (2009) 128–138, https://doi.org/10.1002/FUCE.200800126.

[43] N. Danilov, J. Lyagaeva, A. Kasyanova, G. Vdovin, D. Medvedev, A. Demin, P. Tsiakaras, The effect of oxygen and water vapor partial pressures on the total conductivity of BaCe0.7Zr0.1Y0.2O3–Δ, Ionics (Kiel) 23 (2017) 795–801, https://doi.org/10.1007/S11581-016-1961-1/FIGURES/6.

[44] N. Bonanos, K.S. Knight, B. Ellis, Perovskite solid electrolytes: structure, transport properties and fuel cell applications, Solid State Ionics 79 (1995) 161–170, https://doi.org/10.1016/0167-2738(95)00056-C.

[45] N. Bonanos, Transport study of the solid electrolyte $BaCe_{0.9}Gd_{0.1}O_{2.95}$ at high temperatures, J. Phys. Chem. Solids 54 (1993) 867–870, https://doi.org/10.1016/0022-3697(93)90258-S.

[46] W. Chen, A. Nijmeijer, L. Winnubst, Oxygen non-stoichiometry determination of perovskite materials by a carbonation process, Solid State Ionics 229 (2012) 54–58, https://doi.org/10.1016/j.ssi.2012.10.011.

[47] K. Miyazaki, H. Muroyama, T. Matsui, K. Eguchi, Impact of the ammonia decomposition reaction over an anode on direct ammonia-fueled protonic ceramic fuel cells, Sustain. Energy Fuels 4 (2020) 5238–5246, https://doi.org/10.1039/D0SE00841A.

[48] A. Mohammed Hussain, J.V.T. Høgh, T. Jacobsen, N. Bonanos, Nickel-ceria infiltrated Nb-doped SrTiO3 for low temperature SOFC anodes and analysis on gas diffusion impedance, Int. J. Hydrog. Energy 37 (2012) 4309–4318, https://doi.org/10.1016/j.ijhydene.2011.11.087.

[49] A. Grimaud, F. Mauvy, J.M. Bassat, S. Fourcade, L. Rocheron, M. Marrony, J. C. Grenier, Hydration properties and rate determining steps of the oxygen reduction reaction of perovskite-related oxides as H+-SOFC cathodes, J. Electrochem. Soc. 159 (2012) B683–B694, https://doi.org/10.1149/2.101205jes.

[50] A. Grimaud, F. Mauvy, J. Marc Bassat, S. Fourcade, M. Marrony, J. Claude Grenier, Hydration and transport properties of the Pr2−xSrxNiO4+δ compounds as H+-SOFC cathodes, J. Mater. Chem. 22 (2012) 16017–16025, https://doi.org/10.1039/C2JM31812A.

[51] E. Quarez, Y. Oumellal, O. Joubert, Optimization of the lanthanum tungstate/Pr2NiO4 half cell for application in proton conducting solid oxide fuel cells, Fuel Cells 13 (2013) 34–41, https://doi.org/10.1002/fuce.201200091.

[52] C. Solís, L. Navarrete, J.M. Serra, Study of Pr and Pr and Co doped La2NiO4+δ as cathodes for La5.5WO11.25−δ based protonic conducting fuel cells, J. Power Sources 240 (2013) 691–697, https://doi.org/10.1016/j.jpowsour.2013.05.055.

[55] D. Kek, N. Bonanos, M. Mogensen, S. Pejovnik, Effect of electrode material on the oxidation of H2 at the metal–Sr0.995Ce0.95Y0.05O2.970 interface, Solid State Ionics 131 (2000) 249–259, https://doi.org/10.1016/S0167-2738(00)00669-X.